Radio Science

RESEARCH ARTICLE
10.1029/2020RS007205

A Technique for the Analysis of Radio Occultation Data to Retrieve Atmospheric Properties and Associated Uncertainties

Flavio Petricca[1], **Gael Cascioli**[1], **and Antonio Genova**[1]

[1]Department of Mechanical and Aerospace Engineering, Sapienza University of Rome, Rome, Italy

Key Points:

- We present a method to process raw radio tracking data for the estimation of atmospheric profiles with the associated uncertainties
- Our approach accounts for uncertainties in the spacecraft trajectory that are based on our precise orbit determination (POD) results
- Properties of Mars' atmosphere are retrieved by processing Mars Reconnaissance Orbiter (MRO) unplanned radio occultation data through the proposed technique

Correspondence to
F. Petricca,
flavio.petricca@uniroma1.it

Citation:
Petricca, F., Cascioli, G., & Genova, A. (2021). A technique for the analysis of radio occultation data to retrieve atmospheric properties and associated uncertainties. *Radio Science*, *56*, e2020RS007205. https://doi.org/10.1029/2020RS007205

Received 1 SEP 2020
Accepted 20 MAR 2021

Abstract Among the techniques for atmospheric sounding, radio occultation enables an in depth investigation of vertical profiles from the ionosphere to the troposphere by measuring the radio frequency signal associated to the propagation medium. A precise characterization of the atmospheric layers requires a thorough processing of the raw radio tracking data to estimate the thermodynamic properties of the atmosphere and their related uncertainties. In this work, we present a method to retrieve refractivity, density, pressure, and temperature profiles with the associated uncertainties by analyzing a set of raw radio tracking data occulted by the atmosphere. This technique is also well suited to process two-way Doppler measurements that are not acquired during dedicated occultation campaigns. The NASA mission Mars Reconnaissance Orbiter (MRO) provided a significant amount of radio occultation data that were not planned for atmospheric sounding, but were caused by the spacecraft orbit geometry. Our analysis of one of these occultation profiles with the proposed method allows indicating that MRO occultation datasets provide crucial information regarding Mars' troposphere that can be used as input of general circulation models.

Plain Language Summary A solid technique to investigate the structure of a celestial body atmosphere is based on the analysis of the signals induced by the properties of this medium on the spacecraft radio links that pass through the atmosphere during communications with the Earth. A thorough study of these measurements, that is, radio occultation, allows estimating the vertical profiles of atmospheric density, pressure, and temperature. We present here a method to retrieve these fundamental properties of the atmosphere with their related uncertainties. Radio occultation campaigns are usually planned scientific investigations with dedicated spacecraft operations and requirements. Our method allows processing radio tracking data occulted by the atmosphere that were not accounted for atmospheric studies. The NASA mission Mars Reconnaissance Orbiter (MRO) provided a significant amount of radio data occulted by the Martian atmosphere because of the spacecraft orbit geometry. We processed one of these radio occultation profiles to validate our approach, and to demonstrate that an accurate analysis of this MRO data set helps to enhance our understanding of Mars' troposphere.

1. Introduction

A radio occultation experiment consists in the analysis of the perturbations induced by the atmosphere on an electromagnetic signal propagating through it. The most relevant phenomena that affect a radio signal passing through a medium are refraction and absorption. The bending effects on the signal associated with refraction are related to the refractive index of the atmosphere (i.e., its real part), which in turn is linked to the atmospheric mass density, pressure, and temperature. Refraction causes a Doppler frequency shift of the signal traversing the atmosphere. A time series of frequency Doppler shifts is processed to identify the bending effects and, therefore, the atmospheric thermodynamic profiles, that is, a series of values obtained as a function of the radial distance from the center of the planet.

Several methodologies have been developed to process radio occultation data. An approach is based on ray-tracing algorithms, and it is well suited for oblate refractive environments, such as Jupiter (Lindal et al., 1981), Saturn (Schinder et al., 2015), and Neptune (Lindal, 1992). Radio occultations of terrestrial planets and icy moons of the Solar System have been processed under the assumption of spherical symmetry of their atmospheres. Fjeldbo et al. (1971) proposed this method to obtain a simplified geometry of the

problem with the transmitter, receiver, and target body center of mass in the same plane. This technique has then been expanded by several independent studies. Lipa and Tyler (1979) developed an approach to compute the attainable uncertainty of the atmospheric profiles. Jenkins et al. (1994) suggested different strategies to enable the processing of two-way Doppler data. Withers et al. (2014) introduced relativistic corrections in the expression of the Doppler frequency shift. This second class of methods has been successfully applied to celestial bodies in the Solar System with a negligible oblateness: the Earth (Jensen et al., 2003), Mars (Hinson et al., 1999), Venus (Fjeldbo & Eshleman, 1969; Fjeldbo et al., 1971), Io (Hinson et al., 1998), Titan (Schinder et al., 2012), Europa (Kliore et al., 1997), and Callisto (Kliore et al., 2002).

By using the comprehensive formulation of Withers et al. (2014), we developed a software to process radio occultations. Our method enables the analysis of one-way and two-way Doppler open-loop and closed-loop data through the integration of the radio occultation processing into a precise orbit determination (POD) software. The trajectory of the spacecraft is first retrieved in a POD solution, excluding the data occulted by the atmosphere. The converged trajectory is then used to process the open-loop data through a digital phase-locked loop (PLL) to generate closed-loop data. A POD pass through of this reconstructed data set allows focusing on the atmospheric signal in the Doppler measurements that are processed to retrieve estimates and formal uncertainties of atmospheric density, temperature, and pressure.

This technique enables the analysis of radio occultations to study the atmosphere of terrestrial planets and icy moons. To validate our integrated software, we processed the radio tracking data of the NASA mission Mars Reconnaissance Orbiter (MRO). Because of the spacecraft orbit geometry, the MRO radio tracking are often occulted by the Martian atmosphere before the pericenter (Cascioli et al., 2020). An accurate processing of these data yields fundamental constraints on the Martian tropospheric properties. We present here an MRO radio occultation profile processed through our software, by comparing our results with existing models of the atmosphere of Mars, that is, Mars Global Reference Atmospheric model (GRAM; Justh et al., 2011) and Mars Climate Database (MCD; Forget et al., 1999; Millour et al., 2018).

This study is structured as follows: Section 2 illustrates the theoretical background of the radio occultation investigations; Section 3 provides details on the method developed in this work with a focus on the uncertainty propagation technique adopted; Section 4 shows the results of the application of our method to the MRO radio occultation data.

2. Atmospheric Radio Occultation Investigations

2.1. Geometrical Optics

The refractive and absorptive effects on a radio link passing through a medium with varying optical properties are related to its refractive index real and imaginary parts, respectively (Eshleman, 1973). By observing time-varying radio signal frequency induced by the refraction, a vertical profile of the refractive index real part is retrieved to infer the atmospheric properties.

The theoretical formulation of the radio occulation problem adopted in this work is based on geometrical optics. Radio waves transmitted and received by spacecraft pass through media (i.e., neutral atmosphere and ionosphere), characterized by electrical properties that vary at spatial scales much larger than the electromagnetic wavelength. Therefore, geometrical optics represents in radio occultation a good approximation for the classical electromagnetic theory. The short wavelength assumption allows neglecting diffractive effects and considering the electromagnetic signals as geometric rays (Born & Wolf, 1959). Atmospheric profiles retrieved through the geometrical optics approximations are characterized by vertical resolutions that are limited by diffraction phenomena to the diameter of first Fresnel zone (see Section 4.1). To overcome this limitation and investigate atmospheric structure with small spatial scales, several other theoretical formulations have been proposed. Karayel and Hinson (1997) developed an algorithm based on the scalar diffraction theory that is capable to take into account the diffraction of radio waves. Other procedures based on the radio-holographic method have been developed and applied to radio occultations processing (Jensen et al., 2003).

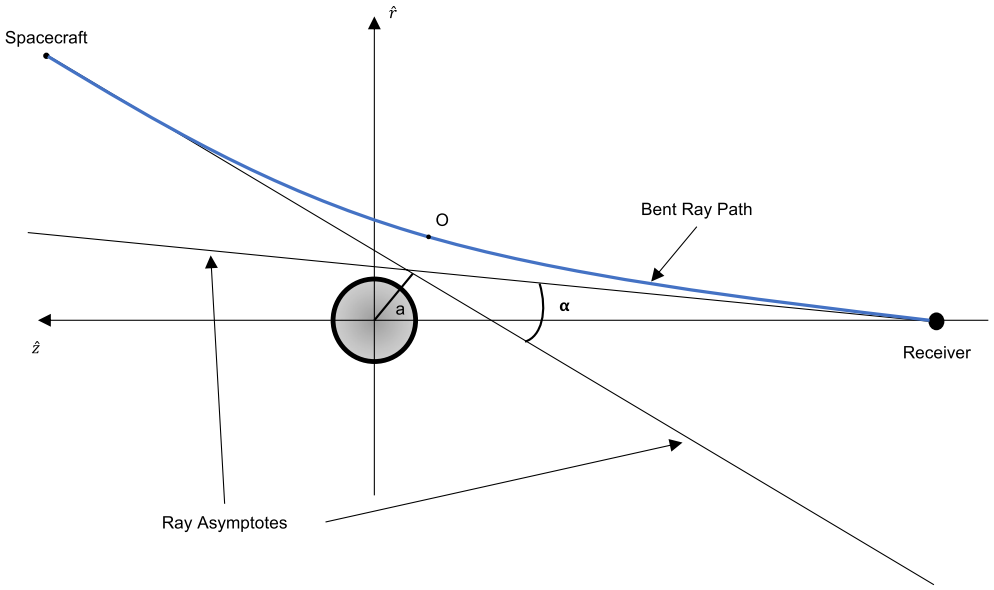

Figure 1. Geometry of a spacecraft radio occultation (adapted from Fjeldbo et al., 1971), where α is the bending angle and a is the impact parameter.

The evolution of a ray propagating through a medium relies on the following (Born & Wolf, 1959):

$$\frac{d}{ds}\left(\mu\frac{dr}{ds}\right)=\nabla\mu \tag{1}$$

where μ is the refractive index of the medium, r is the position vector of a point on the ray, and s is the direction of propagation of the ray. If the ray travels in free space, its path is a straight line. However, in a medium characterized by a varying refractive index the ray bends, leading to a curved path. A further assumption of this work consists in a spherically symmetric atmosphere, so that the atmospheric refractive index distribution only depends on the radial distance from the center of the planet. Since the refractive index of an atmosphere increases with decreasing altitudes above the planetary surface, a ray traversing a spherically symmetric atmosphere increasingly bends as it propagates through, according to Equation 1. The amount by which the ray is bent is called bending angle, it is typically denoted by α (illustrated in Figure 1) and its knowledge can be used to compute the refractive index. The bending angle cannot be directly measured. However, it may be inferred from the frequency shift of the radio signal that is caused by the refraction occurring in the atmosphere.

The geometry of the radio occultation is shown in Figure 1. This representation of the problem geometry with a plane containing the spacecraft, the center of the target body, and the receiver is possible in the assumption of spherically symmetric atmosphere that yields the absence of horizontal refractivity gradients. The bidimensional coordinate frame is $\left(\hat{r},\hat{z}\right)$ with its origin in the center of mass of the target body. The $\hat{r}$ component of the receiver position vector is zero and its $\hat{z}$ component is negative, and both components of the spacecraft position vector are positive. This definition of the problem geometry is fully consistent with the work by Withers et al. (2014).

The ray asymptotes in Figure 1 are defined as the straight lines that the ray follows before traversing the atmosphere (i.e., the direction of the ray as it leaves the transmitter) and after emerging from it (i.e., the direction of the ray entering the receiver). The bending angle α is the angle between the two asymptotes. To determine the relevant properties of the atmosphere, the first step of any radio occultation algorithm is the computation of the bending angle.

Another geometrical quantity introduced in Figure 1 is the impact parameter of the ray, a, that is, the minimum distance between the center of mass of the central body and the asymptote. An important remark is that the impact parameter does not define the point of the ray closest approach to the body, which is named

occultation point and denoted with O in Figure 1. The assumption of spherical symmetry results in the equality between the impact parameters related to the two asymptotes.

2.2. Bending Angles From Radio Frequency Residuals

The first step in the processing of a radio occultation data set consists in the determination of a time series of the bending angle and the associated impact parameter, starting from the knowledge of radio frequency residuals. In this context, the residuals are the differences between the measured radio observable and the radio observable computed by assuming no atmospheric refraction. Previous occultation studies were based on the computation of the predicted observable through preconverged spacecraft trajectory provided by the navigation team. The integration of our radio occultation and POD software results in an accurate computation of the predicted observables because of a refined spacecraft trajectory and the calibration of Earth's troposphere and ionosphere. This method requires highly accurate spacecraft dynamics and measurement modeling to retrieve Doppler residuals converging to the measurement noise (e.g., Additive White Gaussian Noise). During radio link occultation by the central body atmosphere, a clear signature shows an uncompensated Doppler shift caused by the refractive medium. This signal is the data that preserve information regarding the properties of the atmosphere.

In this work, we assume an opposite convention for the sign of the frequency residuals with respect to Withers et al. (2014). The residuals here are positive in the neutral atmosphere and negative in the ionosphere. By definition of relativistic Doppler shift, the ratio between the received (f_{RX}) and transmitted (f_{TX}) frequencies is (Soffel, 1989);

$$\frac{f_{RX}}{f_{TX}} = \frac{1 - \frac{v_{RX} \cdot \hat{n}_{RX}}{c} + \frac{U_{RX}}{c^2} + \frac{{v_{RX}}^2}{c^2}}{1 - \frac{v_{TX} \cdot \hat{n}_{TX}}{c} + \frac{U_{TX}}{c^2} + \frac{{v_{TX}}^2}{c^2}} \tag{2}$$

where the subscripts RX is used for the receiver and TX for the transmitter. v and U are the velocity and the gravitational potential at the location of the transmitter or receiver. The unit vectors $\hat{n}_{RX}$ and $\hat{n}_{TX}$ define the directions of the signal entering the receiver and leaving the transmitter, respectively.

As shown in the work by Withers et al. (2014), Equation 2 is evaluated in two opposite cases that accounts for the signal propagating through the atmosphere and in vacuum, respectively. By differencing these two equations, an explicit expression of the frequency residual is obtained as function of the transmitter and receiver positions and velocities in the considered reference frame, and of the bending angle (see Equation 13 in the work by Withers et al., 2014). The equality of the impact parameter for each asymptote allows obtaining a unique solution for the bending angle and for the impact parameter (see Equations 13 and 17 in the work by Withers et al., 2014).

2.3. Atmospheric Profiles

The determination of the time series of the bending angle and impact parameter is fundamental for deriving a vertical profile of the refractive index μ. Each pair of bending angle and impact parameter values corresponds to a pair of refractive index and radial distance values. The refractive index and the other thermodynamic properties of the atmosphere derived here are computed at the occultation point, where the radial distance is equal to the ray closest distance to the planet, denoted as R_O. From now on we refer to the radial distance of the occultation point simply as radial distance.

As reported in the work by Fjeldbo et al. (1971), the expression that relates the bending angle and impact parameter time series to the refractive index is a special case of the Abel transform;

$$\mu\left(R_O\right) = \exp\left[-\frac{1}{\pi}\int_{\alpha=\alpha_o}^{\alpha=0} \ln\left\{\frac{a(\alpha)}{a_O} + \left[\left(\frac{a(\alpha)}{a_O}\right)^2 - 1\right]^{1/2}\right\} d\alpha\right] \tag{3}$$

where $\alpha_O = \alpha\left(R_O\right)$ and $a_O = a\left(R_O\right)$. The minus sign in the exponential term is due to the convention adopted in our formulation for the sign of the frequency residuals.

To obtain a vertical profile of the refractive index, the radial distance time series is determined by using the Bouguer's law (Born & Wolf, 1959);

$$R_O = \frac{a_O}{\mu\left(R_O\right)} \tag{4}$$

which is valid for a spherical symmetric refractive environment. In presence of oblate atmospheres, the results show substantial divergence from this law (Hubbard, 1975). Note that for thin atmospheres, the refractive index is close to 1 and the impact parameter is approximately equal to the radial distance.

Radio occultation results are usually provided as refractivity profiles, which is typically defined as $\nu = \left(\mu - 1\right) \times 10^6$. In this work, we adopt the alternative definition $\nu = \left(\mu - 1\right)$ (Withers, 2010). The refractivity is positive in the neutral atmosphere and negative in the ionosphere. The two contributions can be analyzed separately, yielding the neutral number density profile (i.e., the number of molecules per cubic meter) in the neutral atmosphere case, and the electron number density profile (i.e., number of electrons per cubic meter) in the ionosphere case.

The ionospheric refractivity profile $\nu_e\left(r\right)$, where r denotes the radial distance from the body center of mass, is related to the electron number density profile $n_e\left(r\right)$ (Eshleman, 1973);

$$\nu_e\left(r\right) = -\kappa_e n_e\left(r\right) = -\frac{e^2}{8\pi^2 m_e \varepsilon_0 f^2} n_e\left(r\right) \tag{5}$$

where κ_e is the refractive volume of one electron, e and m_e are charge and mass of the electron, respectively, ε_0 is the vacuum permittivity, and f is the frequency of the signal. The ionosphere is a dispersive medium and its refractivity depends on the radio frequency. Therefore, the higher is the frequency band in the radio occultation investigation the weaker is the ionosphere contribution to the Doppler shift.

The neutral atmosphere refractivity $\nu_n\left(r\right)$ is related to the neutral number density $n_n\left(r\right)$ (Eshleman, 1973) as follows:

$$\nu_n\left(r\right) = \kappa_n n_n\left(r\right) \tag{6}$$

where κ_n is the mean refractive volume of the neutral atmosphere, obtained as an average of the refractive volume of each constituent of the atmosphere. The mean refractive volume can be easily computed for the atmospheres of celestial bodies in the Solar System with a well-known atmospheric composition.

Being the neutral atmosphere refractivity frequency independant, this medium is nondispersive. Its contribution to the Doppler shift is typically 2 or 3 orders of magnitude larger with respect to the ionosphere (Withers et al., 2014).

The mass density profile $\rho\left(r\right)$ can be obtained from the neutral number density profile through the mean molecular mass m.

$$\rho\left(r\right) = m n_n\left(r\right) \tag{7}$$

This equation is based on the assumption that the atmospheric composition is well known, enabling a straightforward computation of the mean molecular mass.

By assuming the atmosphere in hydrostatic equilibrium, the pressure profile can be retrieved through the equality between the gravitational force exerted by the central body and the pressure gradient of the atmosphere.

$$\frac{\partial p(r)}{\partial r} = -\rho(r)g(r) \tag{8}$$

The gravitational acceleration $g(r)$ may be simply computed by accounting for the gravitational potential monopole term only or higher degrees of the spherical harmonic expansion. The integration of Equation 7 yields the pressure profile as follows:

$$p(r) = p_{bc} + \int_r^{r_{bc}} \rho(r)g(r)dr \tag{9}$$

where p_{bc} and r_{bc} denote the pressure and radial distance at the boundary condition, respectively. This limit is reached when the Doppler shift induced by the atmospheric contribution is below the measurement noise (Hinson et al., 1999). Two independent strategies are adopted to yield the boundary condition. By following the approach by Hinson et al. (1999), p_{bc} may be expressed through the ideal gas law:

$$p_{bc} = n_{bc}kT_{bc} \tag{10}$$

where k is Boltzmann's constant, n_{bc} is the value of the neutral number density at the boundary condition, which is known since $n(r)$ has already been computed, and T_{bc} must be assumed. An independent approach is to obtain the boundary condition from the scale height H of the atmosphere, which can be extracted from the neutral number density profile (Withers & Moore, 2020; Withers et al., 2003, 2014).

$$p_{\mathrm{bc}} = \rho_{\mathrm{bc}} g_{\mathrm{bc}} H. \tag{11}$$

The temperature profile in this second technique is computed through the ideal gas law.

$$T(r) = m\frac{p(r)}{n_n(r)k} \tag{12}$$

3. Methods

The method that we present here is based on the theoretical formulation outlined in Section 2. The final output of our radio occultation algorithm is a set of profiles for the relevant atmospheric properties with the associated uncertainty bounds. The processing scheme is conceptually represented by the pipeline shown in Figure 2. It consists of two main blocks: the POD and the radio occultation processing (ROP).

The POD software enables a very accurate processing of the radio tracking data, including a digital PLL used to generate closed-loop data from open-loop recording. By analyzing the radio tracking data that are not occulted by the atmosphere, the least-squares filter as part of the POD algorithm provides an updated spacecraft trajectory. Therefore, the radio occultation are fed back in a pass-through solution to determine the frequency residuals and the covariance matrix of the spacecraft state (i.e., position and velocity of the spacecraft), which are fundamental for determining the atmospheric profiles and their uncertainties.

The ROP includes the routines devoted to the retrieval of the atmospheric profiles and the associated uncertainties. Our method accounts for an uncertainty determination procedure that is different from those formulated in independent studies (e.g., Lipa & Tyler, 1979; Withers, 2010). In fact, the propagation of the uncertainty here is carried out without the simplification by Withers (2010) and it does not require the linearization of the mathematical model, which was assumed in previous works (e.g., Lipa & Tyler, 1979). Our approach is based on well-established techniques of uncertainty quantification for nonlinear models to account for the measurement accuracy and the spacecraft state uncertainties, which are provided by the POD output covariance matrix.

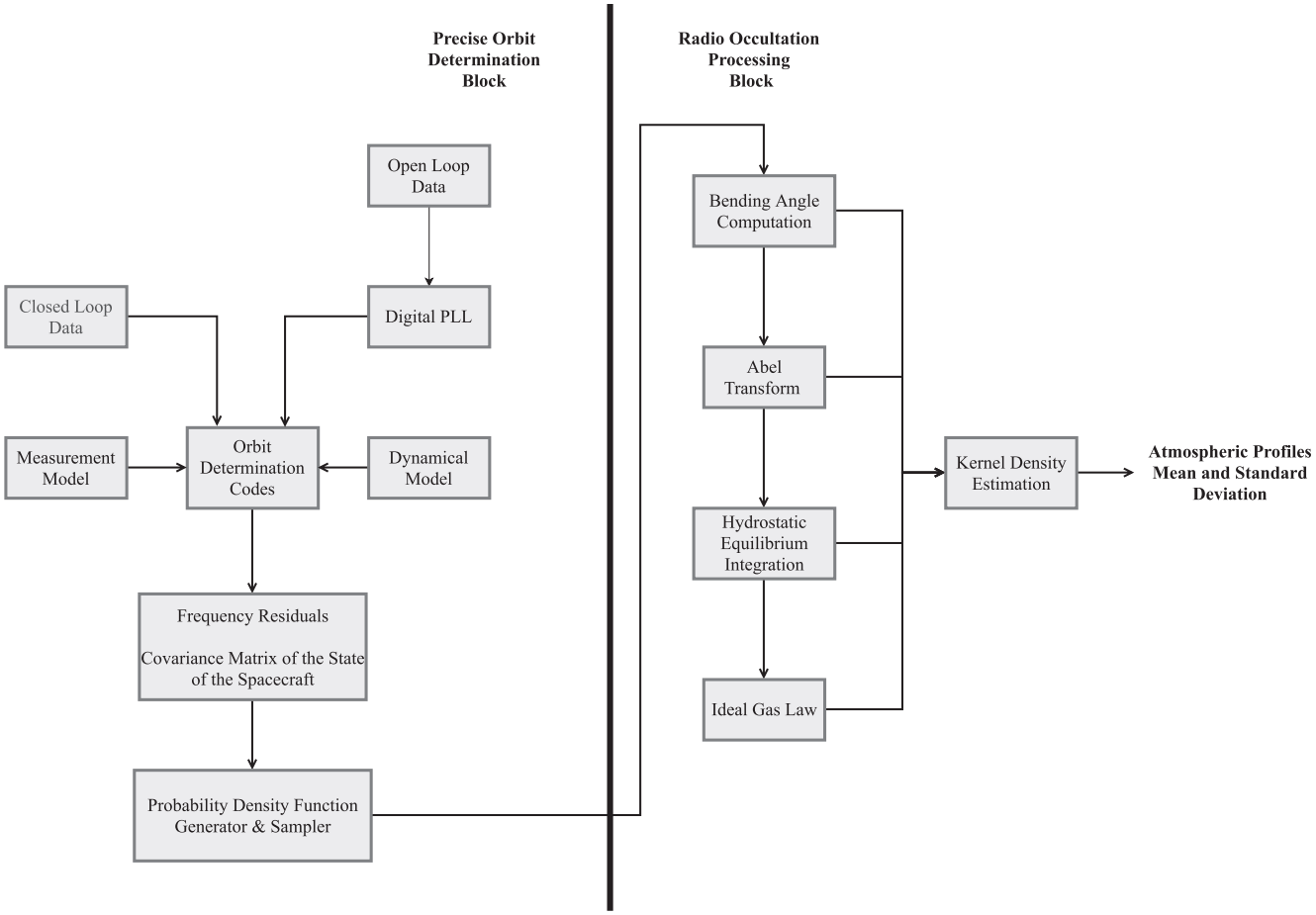

Figure 2. Flow chart of the method developed in this paper. The precise orbit determination (POD) provides the frequency residuals and the state covariance matrix needed in the radio occultation processing (ROP) to derive the atmospheric profiles and the related uncertainties.

3.1. Precise Orbit Determination

An accurate computation of the radio frequency residuals and the spacecraft state covariance matrix is obtained through the POD. The orbit determination processing consists in the minimization of the discrepancy between the actual range rate (i.e., relative velocity between an observing ground station and the spacecraft) measurements collected from the ground station and the predicted observables that are computed by assuming a priori dynamical and measurement modeling. The difference between the observed and computed measurements are the residuals. This minimization process enables the adjustment of the relevant parameters in the dynamical model.

A first POD solution is obtained by ruling out the radio tracking data during atmospheric occultations. This step is required to avoid aliasing in the dynamical model refinement, and to better characterize the atmospheric signal. This approach allows mitigating significant errors in the orbit reconstruction due to the uncompensated atmospheric signal (e.g., Cascioli et al., 2020). The consequent POD solution carried out with the pass through of the entire data set enables the detection of the radio signal associated to the atmospheric refraction.

The radio tracking measurements that are the POD input to determine the frequency residuals for the ROP are collected in two modes: closed-loop ready to be used in the POD being processed through the PLL of the station receiver, and open-loop with the received spectrum down converted and recorded in a preselected bandwidth for post processing by the user (Paik & Asmar, 2011). In the closed-loop mode, the receiver of the ground station makes real-time decisions on determining the signal frequency and power level, while in the open-loop mode, since the entire bandwidth is recorded as raw data, the user process the data to determine

the signal carrier's properties. For occultation investigations, the open-loop mode is typically used because this method provides more flexibility in the processing of the entire data set. The closed-loop recording may present a significant lack of data since the ground receiver PLL is not always able to lock the signal phase for the entire pass, especially at low signal-to-noise ratios (Thomas, 1989). Therefore, a digital PLL is used here to extract the Doppler shift from the open-loop data records.

The post processed Doppler shift observations are then analyzed through the POD least squares filter to adjust the spacecraft trajectory (Tapley et al., 2004). To refine our knowledge of the spacecraft position and velocity, the dynamical equations are precisely modeled accounting for the central body gravitational field and atmosphere, solar, albedo and infrared radiation pressure, third body interaction with other celestial bodies (i.e., planets and the Sun), and general relativity. To precisely retrieve the effects of nonconservative forces, the spacecraft is opportunely modeled including cross sectional areas and reflectivities of its structure. This modeling is based on previous data analyses for gravity investigation (Genova et al., 2016) and for preliminary atmospheric calibration of Doppler data (Cascioli et al., 2020).

These dynamical models used in this work account for the central body gravitational field by expressing it in spherical harmonics expanded to degree and order 120 as estimated by Genova et al. (2016) and for the atmospheric drag by using the Mars GRAM global circulation model (Justh et al., 2011). The estimation methodology used consists in the processing of the tracking data in continuous time span of 1–2 days, called arc. The parameters adjusted in the least-squares fit are called local, if they affect the measurements within a single arc or global and if they affect all the measurements. In this work, the local parameters set contains the state of the spacecraft, the drag coefficient of the spacecraft, and the spacecraft center of mass parameters (Cascioli & Genova, 2020). The global set contains the central body gravitational parameters GM, where G is the gravitational constant and M the mass of the central body. The higher order harmonics are treated as consider parameters, that is their uncertainty is taken into account in the least squares fit, but they are not estimated.

The POD output is a set of Doppler residuals consisting in the atmospheric contribution only, and the spacecraft state covariance matrix that is computed through the least squares solution. The covariance matrix of the spacecraft state is computed in the first POD solution that is retrieved by excluding the radio tracking data occulted by Mars' atmosphere. It is then propagated through the entire POD arc by using the state transition matrix computed with standard techniques for linear dynamical systems theory (Tapley et al., 2004). The exclusion of data collected during the atmospheric occultation has no influence on the state covariance.

3.2. Frequency Residuals Processing

The resulting frequency residuals are then processed through the algorithm described in Section 2. A preliminary calibration of the frequency residuals is applied to average out the Doppler data noise since the Abel transform (Equation 3) requires a monotonic time series of the impact parameter. The data noise may cause indeed deviations of the impact parameter from its natural monotonic behavior, leading to instabilities in the mathematical procedure. The calibration function used to fit the frequency residuals is an exponential function defined by two fitting parameters a, b;

$$\Delta f\left(t\right) = ae^{bt} \tag{14}$$

where Δf is the frequency residual and t represents the time interval from a reference epoch. The result of this calibration is the black line shown in Figure 3, obtained for a radio occultation of the MRO mission which occurred on June 23, 2007 at 06:35:47 UTC. The exponential trend of the residuals is due to the refraction in the neutral atmosphere, reaching a positive peak of 0.528 Hz. The ionospheric contribution to the frequency residuals and to the atmospheric profiles derived is not detected, as it is within the frequency data noise. The calibrated data set is then processed as outlined in Section 2.

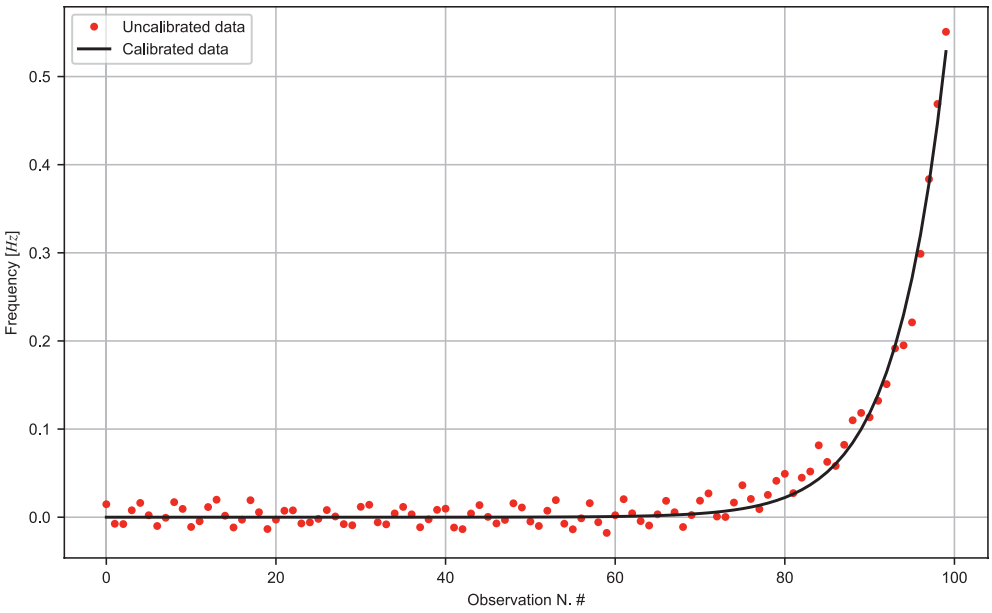

Figure 3. Frequency residuals related to the Mars Reconnaissance Orbiter (MRO) radio occultation occurred on June 23, 2007 at 06:35:47 UTC. The positive peak (0.528 Hz) due to the neutral atmosphere stands out from the Doppler noise, while the ionospheric negative peak is not detectable. The red dots represent the residuals set as generated in the precise orbit determination (POD) process, while the black line is obtained by calibrating this set to prevent undesired effects in the numerical procedure.

3.3. Profiles' Uncertainty Quantification

Several techniques have been developed in radio occultation experiments to provide the uncertainties associated with the derived atmospheric profiles. Withers (2010) introduced the assumption of exponentially decaying refractivity to relate the frequency residuals uncertainty to the refractivity uncertainty. However, this method can only provide simplified analytical expressions for the uncertainties on refractivity, neutral number density, and electron density profiles.

Since the radio occultation problem described in Section 2 is heavily nonlinear, the linear propagation of uncertainty theory cannot be straightforwardly adopted. Lipa and Tyler (1979) proposed a method based on the linearization of the mathematical model that allows involving linear techniques. This method can also be found in recent works on radio occultation experiments (Bocanegra-Bahamòn et al., 2019). However, this kind of approach enables the propagation of the uncertainty related to the frequency residuals only, neglecting the effects due to the spacecraft trajectory mismodeling.

Our method is based on the Monte Carlo class of uncertainty quantification algorithms. This statistical approach for uncertainty quantification allows to propagate the uncertainty on the input variables through nonlinear models. In the context of radio occultation processing, the input variables of the model, which appear in Equation 2, are the position and velocity of the spacecraft (the state) and the frequency residuals. By assuming that these variables are parametrized by a specific probability distribution, N samples are drawn from the distributions for each variable, with N depending on the sampling scheme adopted. If N is large enough, the set of samples provide a statistically significant coverage of the input space. The nonlinear model is then run independently on each sample of the set. Finally, the results are aggregated to obtain a representation of the output variables space, which enables the evaluation of the uncertainties on the output variables, namely the atmospheric profiles. To provide a meaningful statistical description of the output variables, the input space must be well represented, therefore the choice of the sampling scheme and the number of samples N is fundamental.

The setup of this method requires the parametrization of the input variables. These are the components of the position and velocity of the spacecraft projected onto the bidimensional occultation reference frame (see Section 2.1) and the frequency residual. From now on, by "state of the spacecraft" we mean the

four-components vector containing the bidimensional position and velocity of the spacecraft in the occultation frame. Both the state and the frequency residuals are assumed to be normally distributed random variables, with mean given by the values computed in the POD process (i.e., the trajectory and the frequency residuals obtained in the least squares fit of the tracking data). The covariance of the Gaussian probability function (PDF) is given by the covariance matrix of the state of the spacecraft computed in the POD process and by the variance of the frequency measurement. Assuming that the spacecraft state and the frequency residuals are fully uncorrelated, the 5×5 covariance matrix of the PDF is:

$$\Sigma = \begin{bmatrix} \sigma^2_r & \sigma^2_{r,z} & \sigma^2_{r,v_r} & \sigma^2_{r,v_z} & 0 \\ \sigma^2_{r,z} & \sigma^2_z & \sigma^2_{z,v_r} & \sigma^2_{z,v_z} & 0 \\ \sigma^2_{r,v_r} & \sigma^2_{z,v_r} & \sigma^2_{v_r} & \sigma^2_{v_r,v_z} & 0 \\ \sigma^2_{r,v_z} & \sigma^2_{z,v_z} & \sigma^2_{v_r,v_z} & \sigma^2_{v_z} & 0 \\ 0 & 0 & 0 & 0 & \sigma^2_f \end{bmatrix} \tag{15}$$

where σ_r, σ_z, and σ_{v_r}, σ_{v_z} are the standard deviation of the position and velocity of the spacecraft in the $(\hat{r}, \hat{z})$ occultation frame, respectively, and σ_f is the standard deviation of the frequency measurement. The off-diagonal elements represent the covariance terms. The mean of the PDF is given by:

$$\bar{X} = \begin{bmatrix} \overline{r} \\ \overline{z} \\ \overline{v_r} \\ \overline{v_z} \\ \Delta f \end{bmatrix} \tag{16}$$

where $\overline{r}$, $\overline{z}$, and $\overline{v_r}$, $\overline{v_z}$ are the position and velocity of the spacecraft computed in the POD process, respectively, and Δf is the calibrated frequency residual. Therefore, the multivariate Gaussian PDF is:

$$N(X) = \frac{1}{\sqrt{(2\pi)^5 |\Sigma|}} \exp\left(-\frac{1}{2} \left(X - \bar{X}\right)^T \Sigma^{-1} \left(X - \bar{X}\right) \right) \tag{17}$$

The first step of the algorithm is the generation of a multivariate Gaussian PDF (Equation 17) for each observation (PDF generator and sampler block in Figure 2). The frequency observation is aggregated with the corresponding state of the spacecraft into the mean vector $\bar{X}$ and the covariance matrix Σ is propagated forward (Section 3.1). A PDF is generated by using Equation 17 and N samples are drawn from it. This is repeated for each observation to obtain a representation of the input variables space for the entire occultation data set.

The generation of the frequency residuals samples requires a previous step. The frequency residual in the mean vector $\bar{X}$ is obtained by prefitting the residual obtained in POD as outlined in Section 3.2. The Monte Carlo sampling introduces different representations of Gaussian white noise with the RMS of the original data set to the prefitted function, generating N perturbed residuals sets. These N profiles are then individually recalibrated to eliminate any instability that arises in the computation of the Abel transform. This approach provides a fair statistical representation of the uncertainty that accounts possible aliasing due to the calibration.

A random sampling scheme is adopted in Monte Carlo methods to provide statistically solid solutions. However, this scheme requires a remarkable computational effort with a significant amount of samples (i.e., $N \sim 10^6$) to provide a comprehensive sampling of the input five-dimensional PDF. To reduce the computational cost in our method, a Latin hypercube sampling (LHS) scheme was implemented by partitioning the range of each input variable into intervals of equal probability by drawing a single random value for each interval (McKay et al., 1979). Consequently, LHS allows covering the input space in a much more efficient way with a lower number of samples (i.e., $N = 10^4$).

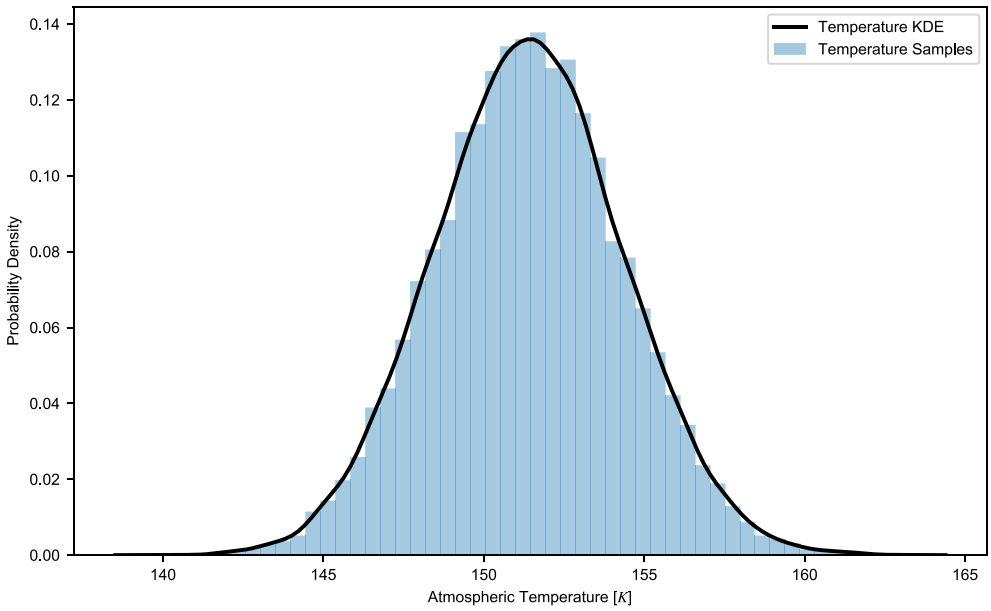

Figure 4. Temperature probability distribution. Each bin of the histogram corresponds to a sample of the temperature. The black line is the temperature probability function (PDF) estimated through the Kernel density estimation (KDE). The estimated PDF has a neat Gaussian shape for every altitude and for each atmospheric property. Consequently, the mean and standard deviation for each value of the profile can be determined straightforwardly.

The resulting set of observables is then processed through the ROP routines to carry out a set of N profiles for the bending angle, the refractivity and the other thermodynamic properties. The output samples are used to estimating the output PDFs through the Kernel density estimation (KDE) (Parzen, 1962).

An example of the output PDF for the atmospheric temperature is reported in Figure 4. The histogram represents the ensemble of samples of the temperature profile determined by using the lowest altitude radio tracking measurement of the MRO occultation profile analyzed. Each output sample is obtained by computing the temperature (as illustrated in Section 2) for each input sample of the model. Therefore, N samples of the output temperature are aggregated and used to estimate the temperature PDF.

The PDF obtained through the KDE can be used to compute the uncertainty of the atmospheric properties at each data point. As shown in Figure 4, the output PDFs are approximately Gaussian distributions leading to a statistically solid computation of their mean and standard deviation.

4. MRO Radio Occultation

The NASA spacecraft MRO has been in a sun-synchronous near-polar orbit about Mars for ∼14 years. This orbit geometry was selected to accomplish the outstanding scientific objectives of the mission (Graf et al., 2005; Zurek & Smrekar, 2007). The spacecraft is equipped with a radio science subsystem to establish telecommunication with ground that enables the acquisition of X-band radio tracking data. This data set has been used to navigate the spacecraft and for geophysical investigations devoted to the determination of the static and time-varying gravity field of Mars (Genova et al., 2016; Konopliv et al., 2016). Although neither the instrumentation nor the orbital configuration were designed to conduct radio occultation campaigns, a significant amount of MRO radio data provides fundamental information on the Martian troposphere, being occulted by the atmosphere during tracking periods before the spacecraft pericenter. For this reason, radio occultation measurements have been frequently performed since 2008, but only two limited sets of observations have been analyzed so far (Hinson et al., 2014).

The radio tracking data of the MRO mission include one-way and two-way Doppler measurements. Radio occultation experiments are commonly conducted through the processing of one-way data because of the two-way data ambiguity induced by uplink and downlink signal paths. The occultation point is then

determined uniquely for one-way data. However, this data type relies on the stability of the onboard ultra-stable oscillator (USO) that is a key instrument of radio occultation investigation (Asmar et al., 2019; Shapira et al., 2016). The MRO USO is characterized by a poor frequency stability with respect to the frequency standards used by the Deep Space Network ground stations, and to other USOs (e.g., Mars Global Surveyor; Tyler et al., 2001). The MRO one-way data show a noise level that is ~5 times larger than two-way data (Genova, 2015). Therefore, our analysis is strictly focused on the MRO two-way range-rate data that include two atmospheric signals detected through uplink and downlink. Since the two links cross region of the Martian atmosphere with a relative distance of few hundred meters only (e.g., Cascioli et al., 2020), we assume that uplink and downlink contributions to the radio signal are equal.

Two-way range-rate data enables the detection of ingress occultations only (i.e., spacecraft approaches the occultation) since the coherent two-way link cannot be established quickly enough for egress occultations (i.e., spacecraft emerges from the planet's limb).

4.1. Retrieval of Atmospheric Profiles

The integration time of the radio tracking data plays a key role in the ROP. A tradeoff between the atmospheric sounding resolution and the Doppler data noise is necessary in the selection of the data temporal sampling to enhance the accuracy of the atmospheric profiles retrieved through the ROP. A shorter integration time leads to a better vertical resolution of the profiles but, on the other hand, causes higher data noise. Furthermore, as shown in the work by Karayel and Hinson (1997), the vertical resolution is limited by diffraction phenomena to the first Fresnel zone diameter, which is equal to $2\sqrt{\lambda D}$, where λ is the wavelength of the tracking signal and D is the distance of the spacecraft from the center of mass of the body. For the MRO case, the Fresnel zone diameter is ~740 m throughout its orbit.

By using a 1 s integration time, MRO radio occultations yield a vertical resolution between 800 m and 1 km, which is greater than the Fresnel zone diameter. Therefore, we used the MRO radio tracking data at 1 s by applying our combined POD and ROP method to a single radio occultation pass of MRO occurred on June 23, 2007. The red dots in Figure 3 represent the frequency residuals as generated in the POD process for this occultation.

The lowest altitude radio tracking data of this pass were occulted by the atmosphere at an altitude above the surface of ~21 km. This represents a reference point for the profiles and the associated uncertainty.

Figure 5 shows the time-series of the bending angle α that is close to zero in the upper layers of the atmosphere since the ionospheric signal is averaged out by the range-rate noise. MRO data provide a detectable signature at radial distances below ~3,440 km reaching a maximum value of 0.0143 mrad at a radial distance of 3,401.5 km from the center of the planet. The estimated uncertainty on the bending angle ranges from 3.23×10^{-6} mrad to 1.67×10^{-4} mrad.

The impact parameter time series is associated with the bending angle time series. Since Mars' atmosphere is thin, its refractive index value is very close to unity and the ray bending is minimal. Therefore, Equation 4 states that the impact parameter is approximately equal to the radial distance.

The combined retrieval of the time series of bending angle and impact parameter allows obtaining the refractivity profile through Equation 3. Figure 6 shows the resulting profiles for the refractivity and the neutral number density. The only contribution to the refractivity profile is indeed given by the neutral atmosphere, which is dominant for Mars at radial distances below ~3,450 km. The maximum value of the refractivity recorded in this occultation is 2.723×10^{-7}, with a corresponding uncertainty of 0.027×10^{-7}, and the maximum neutral number density is $\left(1.509 \pm 0.015\right) \times 10^{22}$ m^{-3}. The neutral number density profile is obtained by simply multiplying the refractivity by the refractive volume (Equation 6), which here is assumed $\kappa_n = 1.804 \times 10^{-29}$ m^3 (Hinson et al., 1999).

The density vertical profile is carried out through Equation 7 by using the neutral number density profile shown in Figure 6 and the mean molecular mass $m = 7.221 \times 10^{-26}$ kg (Hinson et al., 1999).

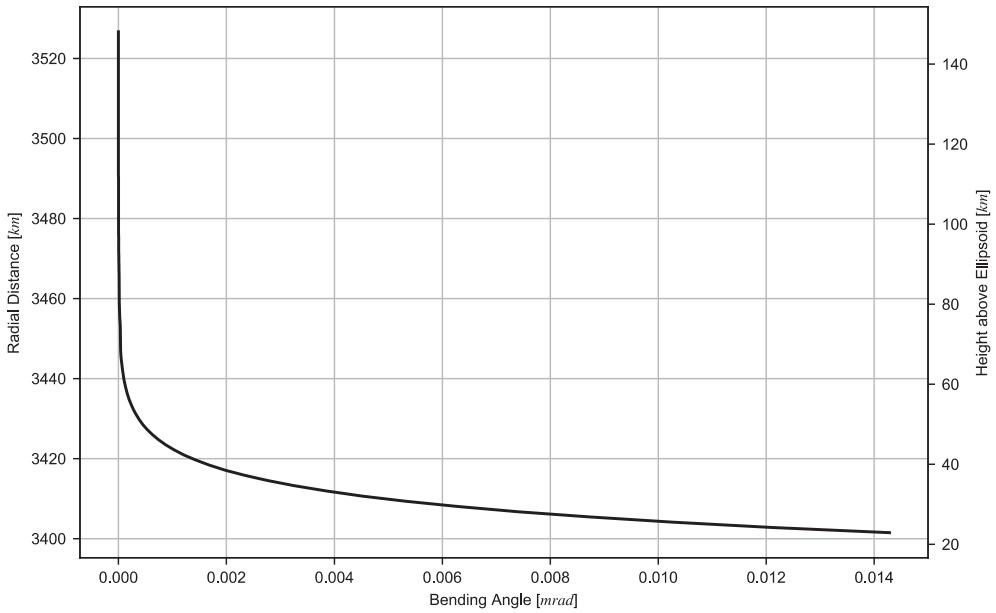

Figure 5. Bending angle vertical profile. The contribution of the neutral atmosphere to the bending angle is positive, while the ionosphere causes negative α. However, the ionospheric signal is within the data noise and not detectable. The bending effects here shown can be entirely attributed to the neutral atmosphere. Above ~65 km, no refraction affects the signal, while a rapid onset is observed at lower altitudes.

To test and validate our results, the density, pressure, and temperature values are reported with the atmospheric predictions based on semi-empirical models. The general circulation models Mars GRAM 2010 and MCD are adopted in this work to compare our profiles with those solutions obtained through Monte Carlo simulations with a combination of theoritical modeling and experimental data.

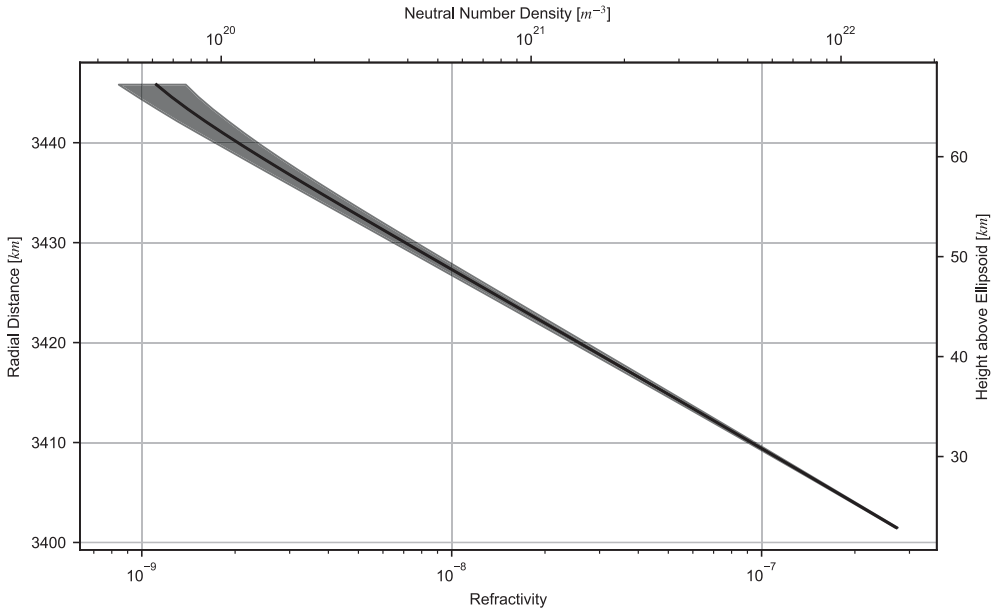

Figure 6. Refractivity and neutral number density profile. As for the bending angle, the only contribution to the refractivity profile is related to the neutral atmosphere. The gray shaded area represents the 1-sigma uncertainty bound for the refractivity profile.

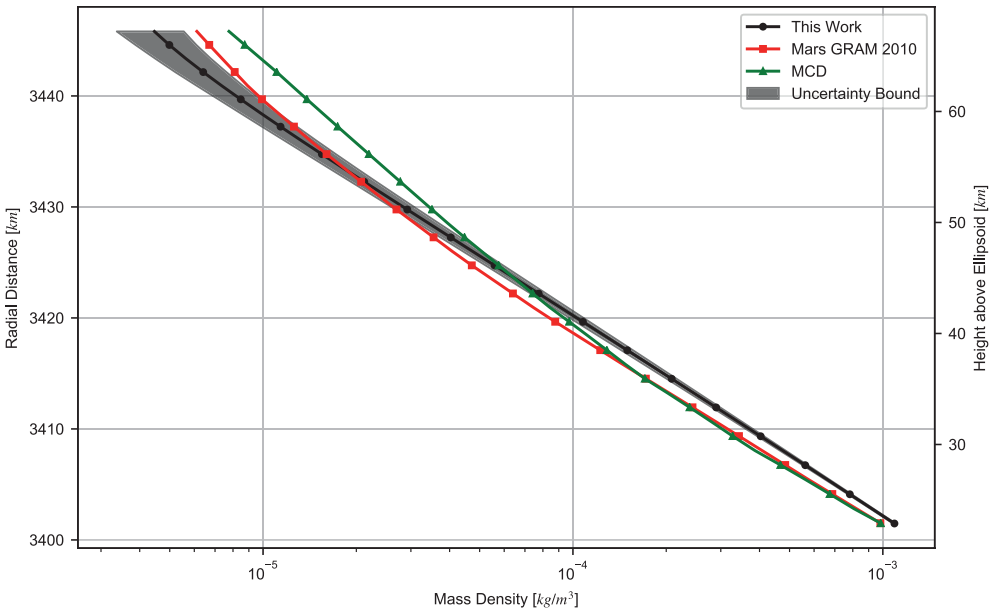

Figure 7. Mass density profile. The profile measured in this work is represented by the black line, while the green and red lines are the numerical predictions of the Mars climate database (MCD) and the Mars Mars global reference atmospheric model (GRAM) 2010, respectively. The uncertainty bound is computed as 1 standard deviation.

The mass density curves shown in Figure 7 indicate consistency between our profile and predictions from the general circulation models, suggesting that our method enables a precise characterization of the atmospheric properties from the data processing. A lower slope in our density trend compared to the semi-empirical models denotes that our estimate of the scale height is slightly lower than predictions. For this occultation, the scale height at ∼21 km results to be 7.81 ± 0.18 km. The estimated value of the density at this altitude is $\left(1.090 \pm 0.011\right) \times 10^{-3}$ kg m^{-3}. These informations represent important constraints that can be provided as input to general circulation models enabling significant improvements of model predictions at altitude ranges, poorly explored by other scientific investigations.

The pressure profiles are reported in Figure 8. The boundary condition needed to integrate the hydrostatic equilibrium equation is computed according to Equation 11, which requires the knowledge of the scale height. The pressure value at the lowest altitude is 31.56 ± 0.77 Pa. The temperature profile (Figure 9) can be simply retrieved from the pressure values by adopting the ideal gas law.

The temperature at the closest distance to the Martian surface (i.e., ∼21 km) is 151.4 ± 2.9 K. By observing the temperature gradient, we are also able to estimate the location of the tropopause. This threshold is the atmospheric layer characterized by an inversion of the temperature gradient, which turns negative in the troposphere. The profile reported here shows that this occurs at an altitude of ∼40–41 km that is in agreement with the vertical structure of Mars' atmosphere (e.g., Sànchez-Lavega, 2011).

The uncertainty in the temperature profile is very sensitive to the data noise reaching a maximum value of ∼7 K.

4.2. Derived Uncertainty Analysis

To better understand the importance of our uncertainty quantification approach, we investigated the impact of the spacecraft trajectory errors on the atmospheric properties uncertainties. Previous methods of radio occultation processing took into account the propagated uncertainty of the frequency measurement only. Figure 10 shows the uncertainty of the temperature profile by not including the spacecraft state covariance matrix (right panel), by accounting for the uncertainty of the spacecraft state (left panel). At low altitudes, the temperature uncertainty is very close to ∼3 K in both cases. However, increasing altitudes

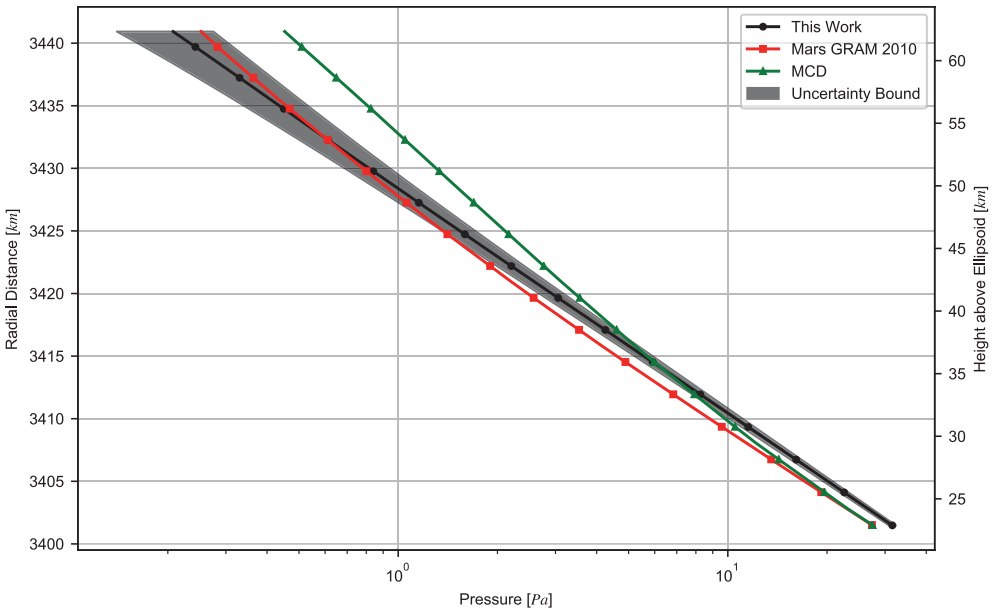

Figure 8. Pressure profile. The estimated profile is consistent with model predictions, represented by the green and the red lines. The uncertainty bound is reported as 1 standard deviation.

lead to larger uncertainties in the case with the full covariance matrix. These results suggest that neglecting the uncertainty associated to the reconstructed spacecraft state affects significantly the uncertainty of the atmospheric profiles. Our method enables, therefore, an accurate estimate of the errors leading to a thorough characterization of the atmospheric profiles. Furthermore, this procedure does not require any further assumption to the model.

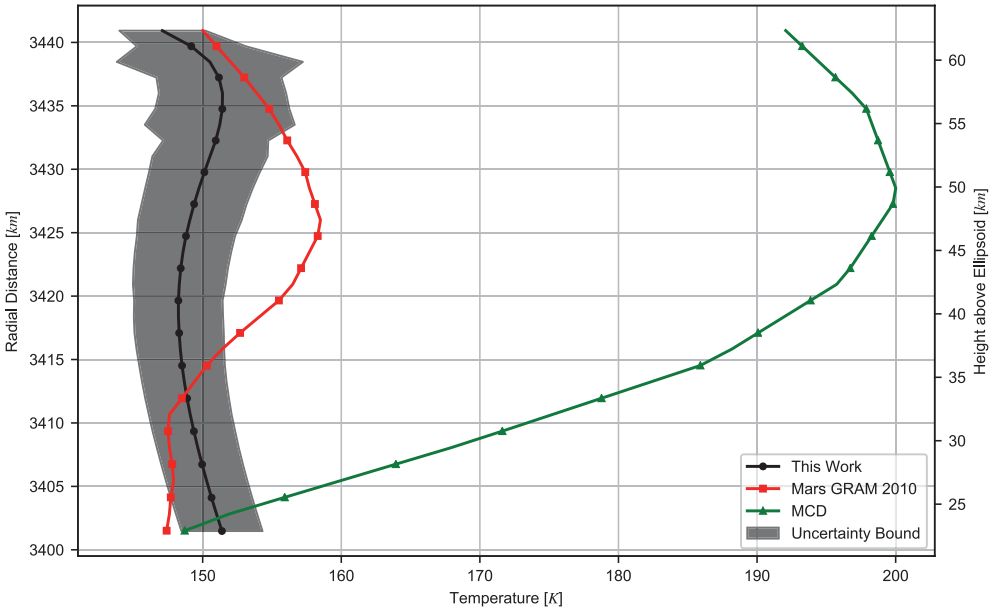

Figure 9. Temperature profile. Our estimated profile is in agreement with the values computed through Mars Mars global reference atmospheric model (GRAM) 2010, while the profile predicted by MCD shows large differences with the other two. The uncertainty grows with altitude as it is very sensitive to the noise in the frequency data. The inversion of the temperature gradient at ∼40 km from the ground, locates the tropopause at that altitude consistently with previous estimates (Sànchez-Lavega, 2011).

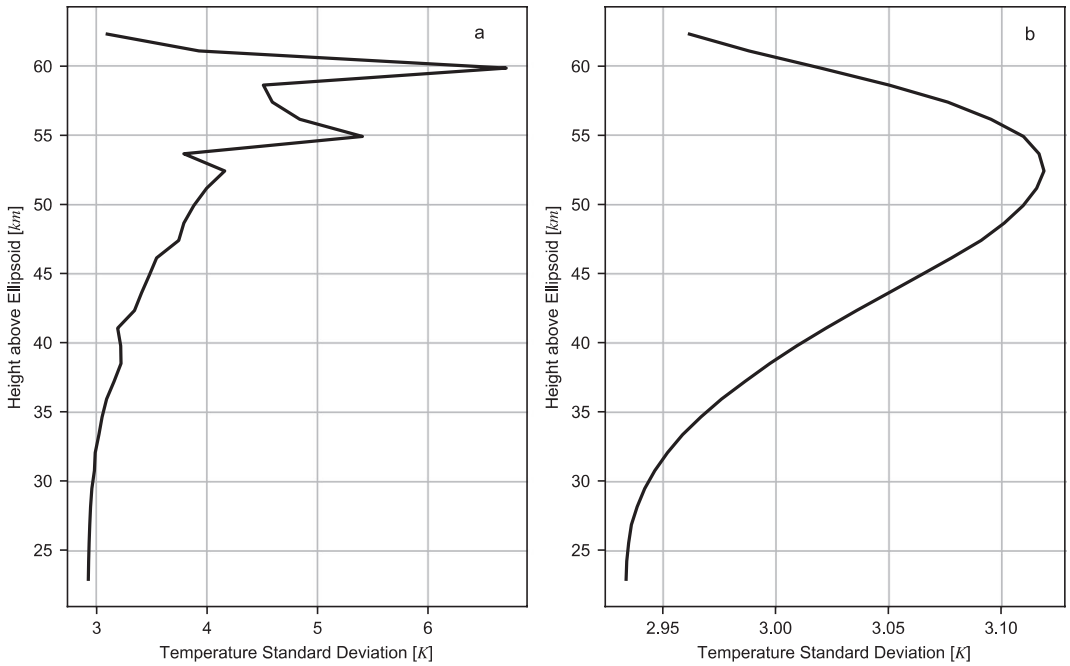

Figure 10. Temperature uncertainty profile computed in two different cases: (a) by using the full precise orbit determination (POD) covariance matrix that stores the uncertainty of the reconstructed spacecraft state; (b) by including only the uncertainty of the Doppler shift measurement.

5. Conclusions

Atmospheric radio occultation represents a powerful scientific investigation to achieve a comprehensive insight into celestial bodies neutral atmospheres and ionospheres. The method presented in this work enables obtaining atmospheric profiles and associated uncertainties by processing raw radio tracking data. Our approach enables the analysis of radio occultations to yield precise information on profiles of the atmospheric properties that are valuable input to general circulation models.

By processing an MRO radio occultation, we presented atmospheric profiles in line with model predictions, based on the Mars GRAM 2010 and MCD. Discrepancies in our pressure and temperature estimates with the values retrieved through both semi-empirical models suggest that MRO radio occultation preserve fundamental information regarding the Martian troposphere.

The technique described in this work is based on the combination of precise orbit determination and radio occultation processing and is well suited to process the amount of MRO occultation data collected during the entire mission. Furthermore, our method provides an accurate characterization of the atmospheric uncertainties by accounting for the standard deviation of the spacecraft position and velocity, which have a significant impact on the determination of the occultation point.

Data Availability Statement

The raw data used in this study are available at https://pds-geosciences.wustl.edu/mro/mro-m-rss-1-magr-v1/mrors_0xxx/. The trajectory and the attitude kernels of the Mars Reconnaissance Orbiter are available at: https://naif.jpl.nasa.gov/pub/naif/MRO/kernels/.

Acknowledgments
This work has been partially funded by grants of the Italian Ministry of Education, University and Research (MIUR). The authors are grateful to Paul Withers (Boston University) for his efforts in sharing the basic techniques used in radio occultation data processing.

References

Asmar, S. W., Lazio, J., Atkinson, D. H., Bell, D. J., Border, J. S., Grudinin, I. S., et al. (2019). Future of planetary atmospheric, surface, and interior science using radio and laser links. *Radio Science*, *54*, 365–377. https://doi.org/10.1029/2018rs006663

Bocanegra-Bahamón, T. M., Molera Calvés, G., Gurvits, L. I., Cimò, G., Dirkx, D., Duev, D. A., et al. (2019). Venus Express radio occultation observed by PRIDE. *Astronomy & Astrophysics*, *624*, 14. https://doi.org/10.1051/0004-6361/201833160

Born, M., & Wolf, E. (1959). *Principles of optics* (p. 952). Pergamon Press.
Cascioli, G., & Genova, A. (2020). Precise orbit determination technique to refine spacecraft mechanical modeling. *Journal of Spacecraft and Rockets*, *58*. https://doi.org/10.2514/1.A34922
Cascioli, G., Petricca, F., & Genova, A. (2020). Mars' atmospheric calibration of radio tracking data for precise orbit determination. *Acta Astronautica*, *177*, 103–110. https://doi.org/10.1016/j.actaastro.2020.07.019
Eshleman, V. R. (1973). The radio occultation method for the study of planetary atmospheres. *Planetary and Space Science*, *21*, 1521–1531. https://doi.org/10.1016/0032-0633(73)90059-7
Fjeldbo, G., & Eshleman, V. R. (1969). Atmosphere of Venus as studied with the mariner 5 dual radio-frequency occultation experiment. *Radio Science*, *4*, 879–897. https://doi.org/10.1029/rs004i010p00879
Fjeldbo, G., Kliore, A. J., & Eshleman, V. R. (1971). The neutral atmosphere of Venus as studied with the mariner V radio occultation experiments. *Astronomical Journal*, *76*, 123–140. https://doi.org/10.1086/111096
Forget, F., Hourdin, F., Fournier, R., Hourdin, C., Talagrand, O., Collins, M., et al. (1999). Improved general circulation models of the Martian atmosphere from the surface to above 80 km. *Journal of Geophysical Research*, *104*, 24155–24175. https://doi.org/10.1029/1999je001025
Genova, A., Goossens, S., Lemoine, F. G., Mazarico, E., Fricke, S. K., Smith, D. E., & Zuber, M. T. (2015). Long-term variability of CO_2 and O in the Mars upper atmosphere from MRO radio science data. *Journal of Geophysical Research: Planets*, *120*, 849–868. https://doi.org/10.1002/2014je004770
Genova, A., Goossens, S., Lemoine, F. G., Mazarico, E., Neumann, G. A., Smith, D. E., & Zuber, M. T. (2016). Seasonal and static gravity field of Mars from MGS, Mars Odyssey and MRO radio science. *Icarus*, *272*, 228–245. https://doi.org/10.1016/j.icarus.2016.02.050
Graf, J. E., Zurek, R. W., Eisen, H. J., Jai, B., Johnston, M. D., & DePaula, R. (2005). The Mars reconnaissance orbiter mission. *Acta Astronautica*, *57*, 566–578. https://doi.org/10.1016/j.actaastro.2005.03.043
Hinson, D. P., Asmar, S. W., Kahan, D. S., Akopian, V., Haberle, R. M., Spiga, A., et al. (2014). Initial results from radio occultation measurements with the Mars reconnaissance orbiter: A nocturnal mixed layer in the tropics and comparisons with polar profiles from the Mars climate sounder. *Icarus*, *243*, 91–103. https://doi.org/10.1016/j.icarus.2014.09.019
Hinson, D. P., Kliore, A. J., Flasar, F. M., Twicken, J. D., Schinder, P. J., & Herrera, R. G. (1998). Galileo radio occultation measurements of Io's ionosphere and plasma wake. *Journal of Geophysical Research*, *103*, 29343–29357. https://doi.org/10.1029/98ja02659
Hinson, D. P., Simpson, R. A., Twicken, J. D., Tyler, G. L., & Flasar, F. M. (1999). Initial results from radio occultation measurements with Mars global surveyor. *Journal of Geophysical Research*, *104*, 26977–27012. https://doi.org/10.1029/1999je001069
Hubbard, W. B., Hunten, D. M., & Kliore, A. (1975). Effect of the Jovian oblateness on Pioneer 10/11 radio occultations. *Geophysical Research Letters*, *2*, 265–268. https://doi.org/10.1029/gl002i007p00265
Jenkins, J. M., Steffes, P. G., Hinson, D. P., Twicken, J. D., & Tyler, G. L. (1994). Radio Occultation studies of the Venus atmosphere with the Magellan spacecraft. *Icarus*, *110*, 79–94. https://doi.org/10.1006/icar.1994.1108
Jensen, A. S., Lohmann, M. S., Benzon, H. H., & Nielsen, A. S. (2003). Full spectrum inversion of radio occultation signals. *Radio Science*, *38*(3), 1040. https://doi.org/10.1029/2002rs002763
Justh, H. L., Justus, C. G., & Ramey, H. S. (2011). Mars-GRAM 2010: Improving the precision of Mars-GRAM. *Paper presented at fourth international workshop on the Mars atmosphere: Modelling and observations*. Paris, France: Laboratoire de Meteorologie dynamique.
Karayel, E. T., & Hinson, D. P. (1997). Sub-Fresnel-scale vertical resolution in atmospheric profiles from radio occultation. *Radio Science*, *32*, 411–423. https://doi.org/10.1029/96rs03212
Kliore, A. J., Anabtawi, A., Herrera, R. G., Asmar, S. W., Nagy, A. F., Hinson, D. P., & Flasar, F. M. (2002). Ionosphere of Callisto from Galileo radio occultation observations. *Journal of Geophysical Reasearch*, *107*. https://doi.org/10.1029/2002JA009365
Kliore, A. J., Hinson, D. P., Flasar, F. M., Nagy, A. F., & Cravens, T. E. (1997). The ionosphere of Europa from Galileo radio occultations. *Science*, *277*, 355–358. https://doi.org/10.1126/science.277.5324.355
Konopliv, A. S., Park, R. S., & Folkner, W. M. (2016). An improved JPL Mars gravity field and orientation from Mars orbiter and lander tracking data. *Icarus*, *274*, 253–260. https://doi.org/10.1016/j.icarus.2016.02.052
Lindal, G. F. (1992). The atmosphere of Neptune: An analysis of radio occultation data acquired with Voyager 2. *The Astronomical Journal*, *103*, 967–982. https://doi.org/10.1086/116119
Lindal, G. F., Wood, G. E., Levy, G. S., Anderson, J. D., Sweetnam, D. N., Hotz, H. B., et al. (1981). The atmosphere of Jupiter: An analysis of the Voyager radio occultation measurements. *Journal of Geophysical Research*, *86*, 8721–8727. https://doi.org/10.1029/ja086ia10p08721
Lipa, B., & Leonard Tyler, G. (1979). Statistical and computational uncertainties in atmospheric profiles from radio occultation: Mariner 10 at Venus. *Icarus*, *39*, 192–208. https://doi.org/10.1016/0019-1035(79)90163-5
McKay, M. D., Beckman, R. J., & Conover, W. J. (1979). Comparison of three methods for selecting values of input variables in the analysis of output from a computer code. *Technometrics*, *21*, 239–245. https://doi.org/10.1080/00401706.1979.10489755
Millour, E., Forget, F., Spiga, A., Vals, M., Zakharov, V., Montabone, L., et al. (2018). The Mars climate database (version 5.3). *Paper presented at scientific workshop: From Mars express to ExoMars*. Madrid, Spain: ESAC.
Paik, M., & Asmar, S. W. (2011). Detecting high dynamics signals from open-loop radio science investigations. *Proceedings of the IEEE*, *99*, 881–888. https://doi.org/10.1109/JPROC.2010.2084550
Parzen, E. (1962). On estimation of a probability density function and mode. *The Annals of Mathematical Statistics*, *33*, 1065–1076. https://doi.org/10.1214/aoms/1177704472
Sánchez-Lavega, A. (2011). *An introduction to planetary atmospheres* (p. 629). Boca Raton, FL: Taylor & Francis.
Schinder, P. J., Flasar, F. M., Marouf, E. A., French, R. G., Anabtawi, A., Barbinis, E., & Kliore, A. J. (2015). A numerical technique for two-way radio occultations by oblate axisymmetric atmospheres with zonal winds. *Radio Science*, *50*, 712–727. https://doi.org/10.1002/2015rs005690
Schinder, P. J., Flasar, F. M., Marouf, E. A., French, R. G., McGhee, C. A., Kliore, A. J., et al. (2012). The structure of Titan's atmosphere from Cassini radio occultations: Occultations from the Prime and Equinox missions. *Icarus*, *221*, 1020–1031. https://doi.org/10.1016/j.icarus.2012.10.021
Shapira, A., Stern, A., Prazot, S., Mann, R., Barash, Y., Detoma, E., & Benn, L. (2016). An Ultra stable oscillator for the 3GM experiment of the JUICE mission. *European frequency and time forum (EFTF)* (pp. 1–5). York, UK. https://doi.org/10.1109/eftf.2016.7477766
Soffel, M. H. (1989). *Relativity in astrometry, celestial mechanics and geodesy*. Springer-Verlag. https://doi.org/10.1007/978-3-642-73406-9
Tapley, B. D., Schutz, B. E., & Born, G. H. (2004). *Statistical orbit determination, United States*. Elsevier. https://doi.org/10.1016/B978-0-12-683630-1.X5019-X
Thomas, J. B. (1989). *An analysis of digital phase-locked loops* (pp. 1–51). Pasadena, CA: Jet Propulsion Laboratory.

Tyler, G. L., Balmino, G., Hinson, D. P., Sjogren, W. L., Smith, D. E., Simpson, R. A., et al. (2001). Radio science observations with Mars Global Surveyor: Orbit insertion through one Mars year in mapping orbit. *Journal of Geophysical Research*, *106*, 23327–23348. https://doi.org/10.1029/2000je001348

Withers, P. (2010). Prediction of uncertainties in atmospheric properties measured by radio occultation experiments. *Advances in Space Research*, *46*, 58–73. https://doi.org/10.1016/j.asr.2010.03.004

Withers, P., & Moore, L. (2020). How to process radio occultation data: 2. From time series of two-way, single-frequency frequency residuals to vertical profiles of ionospheric properties. *Radio Science*, *55*, e2019RS007046. https://doi.org/10.1029/2019RS007046

Withers, P., Moore, L., Cahoy, K., & Beerer, I. (2014). How to process radio occultation data: 1. From time series of frequency residuals to vertical profiles of atmospheric and ionospheric properties. *Planetary and Space Science*, *101*, 77–88. https://doi.org/10.1016/j.pss.2014.06.011

Withers, P., Towner, M. C., Hathi, B., & Zarnecki, J. C. (2003). Analysis of entry accelerometer data: A case study of Mars pathfinder. *Planetary and Space Science*, *51*(9), 541–561. https://doi.org/10.1016/s0032-0633(03)00077-1

Zurek, R. W., & Smrekar, S. E. (2007). An overview of the Mars Reconnaissance Orbiter (MRO) science mission, *Journal of Geophysical Research*, *112*. https://doi.org/10.1029/2006JE002701